

The jet apparent motion and central engine study of *Fermi* blazars

H. B. Xiao,¹★ J. T. Zhu,^{3,5}† J. H. Fan,^{2,4,6}‡ Z. Y. Pei,^{2,4,6} Z. J. Luo,¹ S. H. Zhang,¹

¹Shanghai Key Lab for Astrophysics, Shanghai Normal University, Shanghai 200234, China

²Center for Astrophysics, Guangzhou University, Guangzhou 510006, China

³Department of Physics and Astronomy “G. Galilei”, University of Padova, Padova PD 35131, Italy

⁴Key Laboratory for Astronomical Observation and Technology of Guangzhou, Guangzhou University, Guangzhou 510006, China

⁵Istituto Nazionale di Fisica Nucleare, Padova PD 35131, Italy

⁶Astronomy Science and Technology Research Laboratory of Department of Education of Guangdong Province, Guangzhou 510006, China

Accepted XXX. Received YYY; in original form ZZZ

ABSTRACT

The study of blazar jet has been performed for several decades via VLBI technique, while its generation and propagation stay unclear. In the present work, we compiled a sample of 407 VLBI detected *Fermi* blazars (VFBs) and studied the correlations between apparent velocity ($\log \beta_{\text{app}}$) and jet/accretion disk properties. We found a positive correlation between γ -ray luminosity ($\log L_{\gamma}$) and $\log \beta_{\text{app}}$, the correlation suggests that the apparent motion of jet knot is related to the jet power. The correlations between $\log \beta_{\text{app}}^{\text{max}}$ and the jet radiation power ($\log L_{\text{rad}}$) and between $\log \beta_{\text{app}}^{\text{max}}$ and the jet extended region luminosity at 5 GHz ($\log L_{5\text{GHz}}^{\text{ext}}$), which is an indicator of jet kinetic power, reveal that the knots apparent motion is correlated with both jet radiation power and the kinetic power. But this indication is not held for FSRQs in terms of the correlation $\log L_{5\text{GHz}}^{\text{ext}}$ vs $\log \beta_{\text{app}}^{\text{max}}$. Besides, $\log \beta_{\text{app}}^{\text{max}}$ has a moderate correlation with accretion disk luminosity ($\log L_{\text{Disk}}$) and the normalized accretion disk luminosity $\log (L_{\text{Disk}}/L_{\text{Edd}})$, this may suggest both the power of accretion disk and the accretion rate are critical to generate knots and to accelerate them.

In addition, we found the VFBs have larger average values of γ -ray luminosity ($\log L_{\gamma}$), γ -ray photon index (α_{ph}), and variability index ($\log VI$) than the rest of *Fermi* blazars. Through *Gaussian mixture models* method, we generated a criteria, $\log L_{\gamma} > 45.40$, $\alpha_{\text{ph}} > 2.24$ and $\log VI > 1.71$ to find VFB candidates, selected 228 VFB candidates from the rest of *Fermi* blazar.

Key words: galaxies: active - galaxies: jets - galaxies: kinematics and dynamics - methods: statistical

1 INTRODUCTION

Blazars, an extreme subclass of active galactic nuclei (AGNs), are classified as flat-spectrum radio quasars (FSRQs) and BL Lacertae objects (BL Lac). The former is characterized by strong emission lines, while the latter shows featureless optical spectra or weak emission lines (Scarpa & Falomo 1997). Blazars have a broad electromagnetic emission range (from radio to γ -ray bands) and demonstrate a typical two-hump structure spectral energy distribution (SED) (Abdo et al. 2010; Fan et al. 2016). There are unique and iconic observational properties, rapid and large amplitude variability, high and variable polarization, strong and variable γ -ray emissions and apparent superluminal motion of blazars have been observed and investigated in literature (Wills et al. 1992; Urry & Padovani 1995; Fan 2002; Villata et al. 2006; Fan et al. 2014; Xiao et al. 2015; Gupta et al. 2016; Xiao et al. 2019, 2020; Abdollahi et al. 2020; Fan et al. 2021). These extreme observational properties are mainly due to the presence of a relativistic jet (Blandford & Koenigl 1979), which points to the observer in a small viewing angle

(ϕ) and raises a Doppler beaming effect (Ghisellini et al. 1993; Fan et al. 2013; Pei et al. 2016; Xiao et al. 2020). The Doppler factor ($\delta = [\Gamma(1 - \beta \cos \phi)]^{-1}$, where Γ is the bulk Lorentz factor and β is the jet speed in units of the speed of light, c) is a key parameter in jets since it determines how much of flux is boosted and of timescale is compressed in the observer frame. However, δ can only be determined indirectly because both β and ϕ are unobservable quantities. There are several indicators of the beaming effect that have been introduced in the literature, e.g. core-dominance parameter (Pei et al. 2016, 2020) and apparent superluminal motion of knots (Zhang & Fan 2008; Xiao et al. 2019, 2020).

The study of knots has been performed by VLBI telescopes for decades. These knots, especially the superluminal knots, manifest as localized intensity enhancements in radio images of jets. The enhanced flux refers to a high brightness temperature

$$T = \frac{2c}{\pi k} \frac{S}{\theta_{\text{eq}}^2 \nu^2}, \quad (1)$$

where S is the flux at frequency ν , θ is the angular diameter of a source (Readhead 1994). The T is been observed easily exceed the brightness temperature ($T_{\text{eq}} \approx 5 \times 10^{10}$ K) of jet equipartition, which the power of radiating particles and the power of magnetic field is comparable. While, the brightness temperature is also lim-

★ E-mail: hubing.xiao@shnu.edu.cn

† E-mail: jingtian.zhu@studenti.unipd.it

‡ E-mail: fjh@gzhu.edu.cn

ited by the inverse Compton cooling result in a $T \leq 1.0 \times 10^{12}$ K (Kellermann & Pauliny-Toth 1969). Different authors give discrepant results of the maximum brightness temperature in the rest frame, e.g., Readhead (1994) gave 3×10^{11} K and Liodakis et al. (2018) gave a similar result of 2.78×10^{11} K. The early VLBI observation of brightness temperatures seems to agree with the theoretical brightness temperature limit due to inverse Compton cooling. However, Kellermann (2003) suggested that the agreement was only fortuitous and is a natural consequence of the size of the Earth and the limited range of flux density observed.

In addition to the study of its brightness temperature, the study of knot dynamics is also intriguing. The first superluminal motion was observed on blazar 3C 279 (Cohen et al. 1971), even its explanation was proposed 5 years ago by Rees (1966). Cohen et al. (2007) illustrated the distribution of observed apparent velocity and luminosity is consistent with relativistic beaming models, which has been widely accepted by the following researchers. β_{app} , the apparent velocity of knots of blazar jets, is usually employed to estimate the Doppler factor and the viewing angle (Xiao et al. 2019, 2020) because the superluminal motion and the Doppler boosting are caused by the same geometric effect of jet orientation. Jorstad et al. (2001a) and Kellermann et al. (2004) reported that AGN with γ -ray emission have somewhat higher observed apparent velocity based on EGRET data, and Xiao et al. (2019) found the same result with *Fermi* data. Kellermann et al. (2007) suggested there are no low luminosity sources with fast motions, but the high luminosity sources show a wide range of apparent speeds, this is consistent with the following researchers' work (e.g., Lister et al. 2009; Piner et al. 2012; Xiao et al. 2019). The connection between blazar knots and the γ -ray emission has been addressed two decades ago by Jorstad et al. (2001b) based on the VLBA and EGRET data. This idea has been further confirmed in recent works (Jorstad & Marscher 2016; Jorstad et al. 2017; Weaver et al. 2022) by the VLBV-BU-BLAZAR Program¹, which is a Boston University (BU) γ -ray blazar monitoring program at 43 GHz.

The MOJAVE² (Monitoring of Jets in AGN with VLBA Experiments) program is a long-term program to monitor radio brightness and polarization variations in jets associated with active galaxies visible in the northern sky. They have published features of motions from blazar jets and reported apparent motions in many blazars (Lister et al. 2013, 2018, 2019, 2021).

After the launch of *Fermi* large area gamma-ray space telescope (*Fermi*-LAT), the study of blazars comes to its era of prosperity. The γ -ray detection can be used to investigate the mechanism of the high energetic γ -ray origin. There are five generations of source catalogues that have been released, of which the latest one is the fourth *Fermi*-LAT source catalogue (4FGL_DR2, Abdollahi et al. 2020), in which 3511 blazars have been associated (4LAC_DR2, Ajello et al. 2020). In previous works by (Xiao et al. 2019, 2020), who studied the differences between superluminal blazars with *Fermi* γ -ray detection (FDS) and those without *Fermi* γ -ray detection (non-FDS) by a combined use of MOJAVE and *Fermi*-LAT data. They found that the FDS shows a larger apparent velocity than the non-FDS, indicating a strong beaming effect, and suggested that the apparent velocity is an efficient indicator of the beaming effect (Xiao et al. 2019, 2020). Lister et al. (2019) found a strong correlation between apparent jet velocity and synchrotron peak frequency, with the highest jet velocities being found only in AGNs with low ν_p values, moreover,

Lister et al. (2021) analyzed the parsec-scale jet kinematics of 447 bright radio-loud AGN and suggested the *Fermi*-LAT γ -ray associated AGN in MOJAVE sample tend to have more variable position angles (PAs) than the non-*Fermi* AGNs. Generally, the knots are attributed to the presence of shocks in the collimated plasma outflow (Blandford & Koenigl 1979). However, the correlation between knots' apparent motion and the blazar central engine is barely discussed in previous works, and the nature of how knots form and how they are accelerated still need to be explored. In this work, we aim to investigate the connection between the apparent motion and the jet and accretion disk property and to explore if there are more candidates to be found in the future via VLBI telescopes.

This paper is organised as follows In section 2 we present our sample and describe the data; Our analysis and results will be presented in Section 3; The discussions and further investigation of our results will be presented in Section 4; We summarise our main findings in Section 5. The cosmological parameters $H_0 = 73 \text{ km} \cdot \text{s}^{-1} \cdot \text{Mpc}^{-1}$, $\Omega_m = 0.3$ and $\Omega_\Lambda = 0.7$ are adopted through this paper.

2 DATA ACQUISITION

For the purpose of studying the property of VLBI detected blazars and the correlation between apparent motion and jet and accretion disk. We collect a sample of blazars with available proper motion (μ) or apparent velocity (β_{app}) from literature (Vermeulen et al. 1994; Jorstad et al. 2005; Britzen et al. 2008; Piner et al. 2007; Piner & Edwards 2018; Lister et al. 2019) (see Col. (4), (5), and (6) of Tab. 1). Two rules for data collecting: (1) we use the maximum apparent velocity $\beta_{\text{app}}^{\text{max}}$ for the source with more than one VLBI detected component; (2) we use the MOJAVE (Lister et al. 2019) source as the base sample and omit the same source that comes from other literature because the MOJAVE program is a continuous source monitoring program and provides the latest kinematic measurements with the world's highest resolution telescope VLBA.

Then, we cross-match these sources with 4LAC_DR2 and collect spectrum and variability information (see Col. (11), (12), (13), and (14) of Tab. 1). In total, we compile a sample of 407 *Fermi* blazars with available μ^{max} , in which 372 blazars with available $\beta_{\text{app}}^{\text{max}}$ from literature or calculable $\beta_{\text{app}}^{\text{max}}$ through

$$\beta_{\text{app}} = \frac{\mu}{H_0} \int_1^{1+z} \frac{1}{\sqrt{\Omega_M x^3 + 1 - \Omega_M}} dx \quad (2)$$

(Vermeulen et al. 1994; Zhang & Fan 2008; Xiao et al. 2019). Moreover, we also collect radio flux density (S_ν) from literature (see Col. (7), (8), and (9) of Tab. 1)) and 5 GHz core dominance parameter ($\log R$, Col. (10) of Tab. 1) from Pei et al. (2020). The information of black hole mass (M_{BH} , Col. (15) of Tab. 1) and accretion disk luminosity ($\log L_{\text{Disk}}$, see Col. (16) of Tab. 1) are collected from literature, and the intensity of the inverse Compton peak ($\log F_{\text{IC}}$, see Col. (17) of Tab. 1) is collected from Paliya et al. (2021). For the sake of convenience, these VLBI detected *Fermi* blazars are denoted as VFBs in this work.

¹ <http://www.bu.edu/blazars/BEAM-ME.html>

² <http://www.physics.purdue.edu/MOJAVE/>

Table 1. The sample of *Fermi* blazars

4FGL name	B1950 name	z	ID	μ^{\max} $\mu\text{as/yr}$	Ref	ν GHz	S^{tot} mJy	Ref	log R	Flux1000 $\text{ph} \cdot \text{cm}^{-2} \cdot \text{s}^{-1}$	α_{ph}	Class	VI	$\log(M_{\text{BH}}/M_{\odot})$	$\log L_{\text{Disk}}$ $\text{erg} \cdot \text{s}^{-1}$	$\log F_{\text{IC}}$ $\text{erg} \cdot \text{cm}^{-2} \cdot \text{s}^{-1}$	Ref
(1)	(2)	(3)	(4)	(5)	(6)	(7)	(8)	(9)	(10)	(11)	(12)	(13)	(14)	(15)	(16)	(17)	(18)
J0005.9+3824	0003+380	0.229	2	317 ± 25	L19	15	600.2	L18	1.13	4.25E-10	2.67	F	26.77				
J0006.3-0620	0003-066	0.347	8a	330.4 ± 9.7	L19	15	2351.9	L18	0.26	1.40E-10	2.13	B	20.41	8.93 ± 0.4	44.52 ± 0.15	-12.04	P21
J0009.1+0628	0006+061	1.563	1	134 ± 114	L19	15	185.4	L18		4.77E-10	2.10	B	13.05				
J0014.1+1910	0011+189	0.477	2	159 ± 16	L19	15	133.1	L18	0	2.25E-10	2.28	B	39.85	7.47 ± 0.26	44.32 ± 0.13	-11.65	P21
J0014.8+6118	0012+610		1	13 ± 10	L19					7.91E-10	2.05	U	6.15				

Only five items are listed, this table is available in its entirety in machine-readable forms.

* column (1) 4FGL name; column (2) B1959 Name; column (3) redshift; column (4) feature identification number; column (5) angular proper motion in microarcseconds per year; column (6) reference of proper motion; column (7) frequency; column (8) radio flux density at frequency column (7); column (9) reference of radio flux density;

column (10) core dominance parameter at 5 GHz; column (11) the integral photon flux from 1 to 100 GeV; column (12) the photon spectral index; column (13) classification, 'F' denotes the FSRQ, 'B' denotes the BL Lac, and 'U' denotes the blazars of uncertain type (BCU); column (14) the variability index; column (15) mass of central black hole;

column (16) luminosity of accretion disk; column (17) flux of IC peak; column (18) reference of columns (15), (16) and (17).

C99: Cao & Jiang (1999), C12: Chai et al. (2012) L18: Lister et al. (2018), L19: Lister et al. (2019), P21: Paliya et al. (2021), P14: Piner & Edwards (2014),

P18: Piner & Edwards (2018), Sh12: Shaw et al. (2012), T96: Taylor et al. (1996), X91: Xie et al. (1991), Z12: Zhang et al. (2012).

3 RESULTS

3.1 The correlation between maximum apparent velocity and the luminosity, photon index, and variability index of *Fermi* GeV γ -ray emission

Assuming the γ -ray photons follow a power law function and is expressed as

$$\frac{dN}{dE} = N_0 E^{-\alpha_{\text{ph}}}, \quad (3)$$

where α_{ph} is the photon spectral index, and N_0 can be expressed as $N_0 = N_{(E_L \sim E_U)} \left(\frac{1}{E_L} - \frac{1}{E_U} \right)$, if $\alpha_{\text{ph}} = 2$, otherwise $N_0 = \frac{N_{(E_L \sim E_U)} (1 - \alpha_{\text{ph}})}{E_U^{1-\alpha_{\text{ph}}} - E_L^{1-\alpha_{\text{ph}}}}$, where $N_{(E_L \sim E_U)}$ is the integral photons in units of photons $\cdot \text{cm}^{-2} \cdot \text{s}^{-1}$ in the energy range of $E_L - E_U$, where E_L and E_U correspond to 1 GeV and 100 GeV respectively. The integral flux, F , in units of $\text{GeV} \cdot \text{cm}^{-2} \cdot \text{s}^{-1}$, can be expressed in the form (Fan et al. 2013; Xiao et al. 2015)

$$F = N_{(E_L \sim E_U)} \frac{E_U - E_L}{E_U \times E_L} \ln \frac{E_U}{E_L} \quad (4)$$

for $\alpha_{\text{ph}} = 2$, otherwise

$$F = N_{(E_L \sim E_U)} \frac{1 - \alpha_{\text{ph}}}{2 - \alpha_{\text{ph}}} \frac{(E_U^{2-\alpha_{\text{ph}}} - E_L^{2-\alpha_{\text{ph}}})}{(E_U^{1-\alpha_{\text{ph}}} - E_L^{1-\alpha_{\text{ph}}})}. \quad (5)$$

The γ -ray luminosity is calculated by

$$L_{\gamma} = 4\pi d_L^2 (1+z)^{(\alpha_{\text{ph}}-2)} F, \quad (6)$$

where $d_L = \frac{c}{H_0} \int_1^{1+z} \frac{1}{\sqrt{\Omega_m x^3 + 1 - \Omega_m}} dx$ is a luminosity distance (Komatsu et al. 2011) and $(1+z)^{(\alpha_{\text{ph}}-2)}$ stands for a K -correction.

We calculate γ -ray luminosity for the VFBS and study its correlation with apparent velocity. The upper panel of Figure 1 shows the correlation between $\log L_{\gamma}$ and $\log \beta_{\text{app}}^{\max}$, and gives a linear regression

$$\log L_{\gamma} = (1.68 \pm 0.08) \log \beta_{\text{app}}^{\max} + (44.91 \pm 0.06),$$

and we obtained a correlation coefficient $r = 0.27$ and chance probability $p = 7.1 \times 10^{-8}$ through Pearson analysis (and the Pearson analysis is used to obtain r and p throughout this paper) when the redshift effect is removed.

The middle panel of Fig. 1 shows the correlation between α_{ph} and $\log \beta_{\text{app}}^{\max}$, and gives a linear regression

$$\alpha_{\text{ph}} = (0.15 \pm 0.02) \log \beta_{\text{app}}^{\max} + (2.22 \pm 0.02),$$

with a $r = 0.33$ and $p = 3.1 \times 10^{-11}$.

The variability index (VI) is, a parameter that indicates the level of variability, introduced in the works of *Fermi Collaboration*, e.g. Nolan et al. (2012) used a simple likelihood ratio to test the variability for the two-year data of *Fermi* observation and Acero et al. (2015) applied the same method to the four-year data. However, the *Fermi Collaboration* added a second term (see in Eq. 7) corrects (in the Gaussian limit) for the different weights between the full analysis and that in 1 yr intervals, the average flux from the light curve F_{av} can differ somewhat from the flux in the total analysis F_{glob} in the 4FGL, expressed as:

$$VI = 2 \sum_i \log \left[\frac{\mathcal{L}_i(F_i)}{\mathcal{L}_i(F_{\text{glob}})} \right] - \max(\chi^2(F_{\text{glob}}) - \chi^2(F_{\text{av}}), 0), \quad (7)$$

$$\chi^2(F) = \sum_i \frac{(F_i - F)^2}{\sigma_i^2}, \quad (8)$$

where F_i are the individual flux values, $\mathcal{L}_i(F)$ is the likelihood in the interval i assuming flux F , and σ_i are the errors on F_i , F_{av} is the average flux over one-year interval light curve and F_{glob} is the flux obtained from a global fit. A source would be considered to show probable variability if $VI > 18.48$, corresponding to 99% confidence in a χ^2 distribution, at GeV band (Abdollahi et al. 2020). In the bottom panel of Figure 1 shows the correlation between $\log VI$ and $\log \beta_{\text{app}}^{\max}$, and gives a linear regression

$$\log VI = (0.32 \pm 0.07) \log \beta_{\text{app}}^{\max} + (1.94 \pm 0.07),$$

with a $r = 0.21$ and $p = 2.7 \times 10^{-5}$.

3.2 The correlation between maximum apparent velocity and black hole mass, accretion disk luminosity, and the normalized accretion luminosity

The black hole mass is estimated in several ways. The typical tactic is to use the virial theorem and estimate the central black hole mass through

$$M_{\text{BH}} \approx rv^2/G, \quad (9)$$

where v is the velocity dispersion of matter at distance r . The velocity dispersion can be derived from spectroscopic study and expressed as $v = fv_{\text{FWHM}}$, where v_{FWHM} is the FWHM of the broad emission line and f is, an geometry and kinematics dependent factor, on the order of unity (Peterson et al. 1999, 2000; McLure & Dunlop 2001; Vestergaard 2002). The distance r can be well determined by the

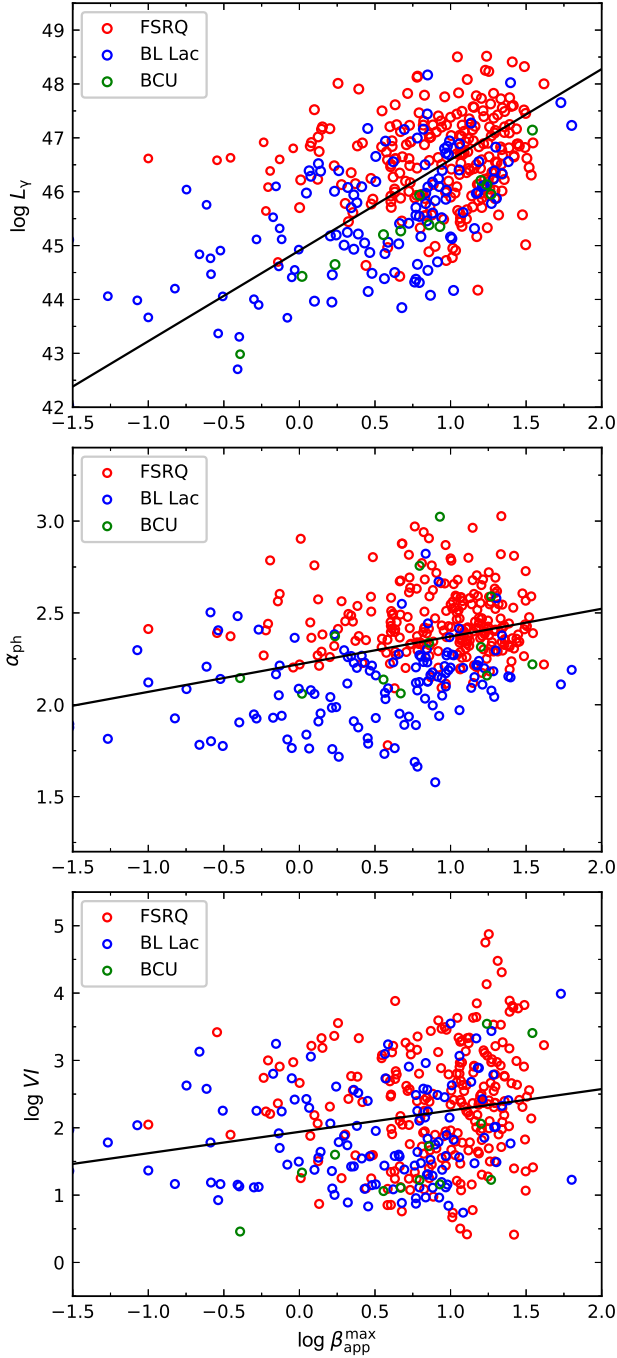


Figure 1. The correlations of $\log L_\gamma$, α_{ph} and $\log VI$ against $\log \beta_{\text{app}}^{\text{max}}$ for the VFBs. The FSRQs in red, the BL Lacs in blue, and the BCUs in green.

reverberation mapping, and so that the ‘Size-Luminosity Relation’ (Kaspi et al. 2000). Thus, the virial M_{BH} can be calculated using the following equation (Shen et al. 2011; Paliya et al. 2021):

$$\log \left(\frac{M_{\text{BH}}}{M_\odot} \right) = a + b \log \left(\frac{\lambda L_\lambda}{10^{44} \text{ erg} \cdot \text{s}^{-1}} \right) + 2 \log \left(\frac{\text{FWHM}}{\text{km} \cdot \text{s}^{-1}} \right), \quad (10)$$

where λL_λ is the continuum luminosity at given wavelength, e.g., 5100 Å for H β , 3000 Å for Mg II and 1350 Å for C IV. The coefficients a and b can be taken from McLure & Dunlop (2004) and Vestergaard & Peterson (2006). Similarly, a stellar velocity dispersion is used to estimate M_{BH} (Gültekin et al. 2009). Moreover, the host galaxy bulge luminosity is also suggested to be the estimator of M_{BH} . Paliya et al. (2021) utilized these three methods and calculated M_{BH} for a sample of *Fermi* blazars, in which 269 sources in our sample are included. The upper panel of Fig. 2 shows the correlation between $\log (M_{\text{BH}}/M_\odot)$ and $\log \beta_{\text{app}}^{\text{max}}$, gives a linear regression

$$\log (M_{\text{BH}}/M_\odot) = (0.12 \pm 0.06) \log \beta_{\text{app}}^{\text{max}} + (8.57 \pm 0.06),$$

with $r = 0.12$ and $p = 0.05$.

The accretion disk luminosity (L_{Disk}) is usually derived either from the SED modelling of the blue bump or from the broad emission-line luminosity ($L_{\text{BLR}} = 0.1 L_{\text{Disk}}$), where the 0.1 is the broad emission-line region (BLR) covering factor. The L_{BLR} can be calculated by using the following equation

$$L_{\text{BLR}} = \sum_i L_i \cdot \frac{\langle L_{\text{BLR, rel}} \rangle}{\sum_i L_{i, \text{rel}}}, \quad (11)$$

where $\langle L_{\text{BLR, rel}} \rangle = 556$, L_i is observed line luminosity, and $L_{i, \text{rel}}$ is relative line luminosity. The Ly α as a reference flux that contributed to 100, the relative weight of H α , H β , Mg II and C IV lines to 77, 22, 34, and 63, the total broad emission-line flux is then fixed as 556 (Celotti et al. 1997; Francis et al. 1991; Paliya et al. 2021; Xiao et al. 2022). Paliya et al. (2021) utilized the methods and calculated L_{Disk} or 3σ upper limits for a sample *Fermi* blazars, in which 254 sources of our sample are included.

In the middle panel of Fig. 2, the plot shows a positive correlation between $\log L_{\text{Disk}}$ and $\log \beta_{\text{app}}^{\text{max}}$ gives a linear regression

$$\log L_{\text{Disk}} = (1.59 \pm 0.10) \log \beta_{\text{app}}^{\text{max}} + (44.22 \pm 0.08),$$

with a correlation coefficient $r = 0.32$ and chance probability $p = 1.1 \times 10^{-7}$ when the redshift effect is removed.

The Eddington luminosity L_{Edd} is a function of Eddington accretion rate (\dot{M}_{Edd}) and is expressed as $L_{\text{Edd}} = \dot{M}_{\text{Edd}} c^2 = 1.26 \times 10^{38} (M/M_\odot) \text{ erg} \cdot \text{s}^{-1}$. We calculate L_{Edd} for the sources with black hole mass in our sample, analysis the correlation between $\log (L_{\text{Disk}}/L_{\text{Edd}})$ and $\log \beta_{\text{app}}^{\text{max}}$ as shown in the lower panel of Fig. 2, in which a linear regression gives

$$\log (L_{\text{Disk}}/L_{\text{Edd}}) = (0.71 \pm 0.11) \log \beta_{\text{app}}^{\text{max}} - (1.88 \pm 0.11),$$

with $r = 0.40$ and $p = 4.8 \times 10^{10}$.

3.3 The distributions of VFBs and the rest of *Fermi* blazars

The 4FGL_R2 contains 3511 blazars, in which 2009 sources with available redshift in literature or from NED. The redshift ranges from 0.00351 (4FGL J1248.3+5820/PG 1246+586) to 4.162481 (4FGL J0929.3+5014/GB6 J0929+5013) with an average value of $\langle z^{\text{VFB}} \rangle = 0.95 \pm 0.68$ for the VFBs, while redshift ranges from 0.00001 (4FGL J1113.8+1528/2MASS J11135586+1528058) to 6.3952 (4FGL J1233.7-0144/NVSS J123341-014426) with an average value of $\langle z^{\text{R}} \rangle = 0.79 \pm 0.76$ for the rest of *Fermi* blazars, as shown in Fig. 3.

We calculate the γ -ray luminosity for both the VFBs and the rest of *Fermi* blazars, and illustrate it in the upper panel of Fig. 4. The luminosity of the VFBs ranges from 42.04 to 48.51 with an average value ($\log L_\gamma^{\text{VFB}} = 46.20 \pm 1.07$, and ranges from 35.22 to 48.76 with an average luminosity of the rest blazars is $\langle \log L_\gamma^{\text{R}} \rangle = 45.24 \pm 1.42$.

Anderson-Darling (A-D) test is applied to test if $\log L_\gamma^{\text{VFB}}$ and $\log L_\gamma^{\text{R}}$ are from the same distribution. The A-D test gives a statistic 111.3 greater than the critical statistic 6.5 for significance level 0.1%, the null hypothesis that the two samples come from the same distribution. Thus we can state the γ -ray luminosity distributions for the VFBs is different from that of the rest *Fermi* blazars, and the VFBs have a larger average γ -ray luminosity than the rest.

The photon index (α_{ph}) ranges from 1.58 to 3.03 with an average value $\langle \alpha_{\text{ph}}^{\text{VFB}} \rangle = 2.33 \pm 0.25$ for the VFBs; and α_{ph} ranges from 1.40 to 3.63 with an average value $\langle \alpha_{\text{ph}}^{\text{R}} \rangle = 2.21 \pm 0.30$ for the rest *Fermi* blazars, as shown in the middle panel of Figure 4. An A-D test is applied to the distributions of $\alpha_{\text{ph}}^{\text{VFB}}$ and $\alpha_{\text{ph}}^{\text{R}}$, the A-D test gives a statistic 47.0 greater than the critical statistic 6.5 for significance level 0.1%, suggesting $\alpha_{\text{ph}}^{\text{VFB}}$ and $\alpha_{\text{ph}}^{\text{R}}$ are from different distributions, and the VFBs have larger photon index than the rest of *Fermi* blazars.

In our sample, $\log VI$ ranges from 0.41 to 4.88 with an average value $\langle \log VI^{\text{VFB}} \rangle = 2.14 \pm 0.84$ for the VFBs; $\log VI$ ranges from 0.16 to 4.13 with an average value $\langle \log VI^{\text{R}} \rangle = 1.30 \pm 0.50$ for the rest of *Fermi* blazars, seen in the bottom panel of Fig. 4. An A-D test is applied to the distributions of $\log VI^{\text{VFB}}$ and $\log VI^{\text{R}}$, the A-D test gives a statistic 327.9 greater than the critical statistic 6.5 for significance level 0.1%, suggesting $\log VI^{\text{VFB}}$ and $\log VI^{\text{R}}$ are from different distributions, and the VFBs have larger variability index than the rest of *Fermi* blazars.

4 DISCUSSION

4.1 The apparent motion and the central engine of blazars

We have studied the correlation between maximum apparent velocity and the GeV γ -ray for the VFBs in our sample. It is shown that a positive correlation between $\log L_\gamma$ and $\log \beta_{\text{app}}^{\text{max}}$. Before discussing the implications of this correlation, there is a caveat to note, concerning the important Doppler beaming effect. Blazar γ -ray emission has been proved to be boosted due to a beaming effect (Xiao et al. 2015; Pei et al. 2016; Fan et al. 2016; Xiao et al. 2019, 2020; Zhang et al. 2020; Paliya et al. 2021). We extract the L_γ regarding the Doppler beaming effect according to

$$L_\gamma^{\text{in}} = L_\gamma^{\text{ob}} / \delta^{q+1}, \quad (12)$$

where δ is the Doppler factor that we calculated with the approach suggested in Zhang et al. (2020), $q = 2 + \alpha$ for a continuous jet emission (or $q = 3 + \alpha$ for a discrete jet emission), and $\alpha = (\alpha_{\text{ph}} - 1)$ is a spectral index $f_\nu \propto \nu^{-\alpha}$. A correlation of the intrinsic γ -ray luminosity $\log L_\gamma^{\text{in}}$ against $\log \beta_{\text{app}}^{\text{max}}$ is shown in Fig. 5, the linear regression gives

$$\log L_\gamma^{\text{in}} = (1.84 \pm 0.10) \log \beta_{\text{app}}^{\text{max}} + (41.72 \pm 0.08),$$

with a $r = 0.26$ and $p = 5.8 \times 10^{-7}$ for the case of $q = 2 + \alpha$ when the redshift effect is removed; and

$$\log L_\gamma^{\text{in}} = (2.02 \pm 0.13) \log \beta_{\text{app}}^{\text{max}} + (40.65 \pm 0.10),$$

with a $r = 0.23$ and $p = 1.0 \times 10^{-5}$ for the case of $q = 3 + \alpha$ when the redshift effect is removed. Obviously, the positive correlations ($\log \beta_{\text{app}}^{\text{max}}$ vs $\log L_\gamma$ and $\log \beta_{\text{app}}^{\text{max}}$ vs $\log L_\gamma^{\text{in}}$) indicating that the motion of knots may correlate with the jet central engine.

In general, the entire jet power (P_{jet}) is attributed to the radiation power (P_{rad}) and the kinetic power (P_{kin}), which is responsible for jet nonthermal radiation and its propagation, respectively. It is possible to estimate P_{rad} and P_{kin} through several methods, among

of which the broadband SED fitting based on the simultaneous data gives both the kinetic and the radiation power (Ghisellini et al. 2014; Tan et al. 2020). Ghisellini & Tavecchio (2010) and Ghisellini et al. (2014) carried out the radiation power

$$P_{\text{rad}} = 2f \frac{\Gamma^2 L_{\text{jet}}^{\text{bol}}}{\delta^4}, \quad (13)$$

where the factor 2 counts for two-sided jets, f equals 16/5 for the case of SSC process (mostly BL Lacs), $f = 4/3$ and replace δ^4 with $\delta^4(\delta/\Gamma)^2$ for the case of EC process (mostly FSRQs). We can calculate P_{rad} with two assumptions. Firstly, Γ is believed to be equal to δ for blazars because of the small viewing angle (Ghisellini & Tavecchio 2010; Ghisellini et al. 2014; Xiong & Zhang 2014; Zhang et al. 2020; Xiao et al. 2022). Secondly, the L_γ has been involved in calculating δ through the method in Zhang et al. (2020), thus for the purpose of avoiding degeneration between L_γ and δ , seen in Eq. 13, the $L_{\text{bol}}^{\text{jet}}$ is represented by the inverse Compton peak luminosity L_{IC} rather than L_γ as used in previous works (Ghisellini & Tavecchio 2010; Ghisellini et al. 2014; Xiong & Zhang 2014; Zhang et al. 2020). The peak luminosity of inverse Compton is given by $L_{\text{IC}} = 4\pi d_L^2 F_{\text{IC}}$, where F_{IC} , the inverse Compton peak flux, is obtained from Paliya et al. (2021).

Cavagnolo et al. (2010) suggested that the jet kinetic power is able to inflate the X-ray cavities or bubbles in different systems including giant elliptical galaxies and cD galaxies (Type cD galaxy, a subtype of type-D giant elliptical galaxy), and proposed to evaluate the kinetic power $P_{\text{kin}} = P_{\text{cav}}$. However, this method is only limited to a small number of sources at present. It is known that the luminosity of extended region of radio jet, which is believed to be less Doppler boosted, is related to jet kinetic power (Rawlings & Saunders 1991; Willott et al. 1999; Cavagnolo et al. 2010; Meyer et al. 2011), $P_{\text{rad}} = \eta (L_{5\text{GHz}}^{\text{ext}})^\kappa$. Through The factor κ and η are given in discrepancy in literature due to the different sizes and source types of sample (Cavagnolo et al. 2010; Meyer et al. 2011), the $\log L_{5\text{GHz}}^{\text{ext}}$ scales with the $\log P_{\text{rad}}$ in the logarithmic space. We collect the total radio flux density from literature (Taylor et al. 1996 at 5 GHz, Piner & Edwards 2014 at 8.4 GHz, and Lister et al. 2018 at 15 GHz) and we convert the data at other frequencies to 5 GHz by assuming that

$$S_{5\text{GHz}}^{\text{core}} = S_\nu^{\text{core}} \text{ and } S_{5\text{GHz}}^{\text{ext}} = S_\nu^{\text{ext}} \left(\frac{\nu}{5\text{GHz}} \right)^{\alpha_{\text{ext}}}, \quad (14)$$

where the total radio flux is the sum of the flux of core and the flux of the extended region, $S^{\text{tot}} = S^{\text{core}} + S^{\text{ext}}$, the $\alpha_{\text{ext}} = 0.75$ and $\alpha_{\text{core}} = 0$ (Fan et al. 2011; Pei et al. 2016, 2019, 2020). Together with the radio core dominance parameter at 5 GHz

$$R = \left(\frac{S^{\text{core}}}{S^{\text{ext}}} \right) (1+z)^{\alpha_{\text{core}} - \alpha_{\text{ext}}}, \quad (15)$$

that we collect from Pei et al. (2020), we obtain $S_{5\text{GHz}}^{\text{ext}}$ and calculate $\log L_{5\text{GHz}}^{\text{ext}}$. The correlations of $\log P_{\text{rad}}$ and $\log L_{5\text{GHz}}^{\text{ext}}$ against $\log \beta_{\text{app}}^{\text{max}}$ are illustrated in Fig. 6 and linear regression results are listed in Tab. 2. Positive correlations of $\log P_{\text{rad}}$ vs $\log \beta_{\text{app}}^{\text{max}}$ and $\log L_{5\text{GHz}}^{\text{ext}}$ vs $\log \beta_{\text{app}}^{\text{max}}$ are found for blazars. The positive correlation of $\log P_{\text{rad}}$ vs $\log \beta_{\text{app}}^{\text{max}}$ holds for both FSRQs and BL Lacs when we consider them independently, while the positive correlation of $\log L_{5\text{GHz}}^{\text{ext}}$ vs $\log \beta_{\text{app}}^{\text{max}}$ only hold for BL Lacs. It is found that the motion of jet knots is significantly correlated with jet radiation power for both FSRQs and BL Lacs, however, the motion of jet knots is correlated with the kinetic power only for BL Lacs.

Moreover, we have investigated the correlation between apparent motion and black hole mass, luminosity of accretion disk, and normalized disk luminosity, seen in Fig. 2. Our results suggest

Table 2. The correlation of $\log P_{\text{rad}}$ and $\log L_{5\text{GHz}}^{\text{ext}}$ against $\log \beta_{\text{app}}^{\text{max}}$

Type	class	($a \pm \Delta a$)	($b \pm \Delta b$)	N	r	p
$\log P_{\text{rad}}$ v.s $\log \beta_{\text{app}}^{\text{max}}$	All	1.78 ± 0.12	43.62 ± 0.10	249	0.29	5.0×10^{-6}
	FSRQs	1.34 ± 0.12	44.12 ± 0.11	207	0.19	6.9×10^{-3}
	BL Lacs	1.59 ± 0.19	43.20 ± 0.07	42	0.34	0.03
$\log L_{5\text{GHz}}^{\text{ext}}$ v.s $\log \beta_{\text{app}}^{\text{max}}$	All	2.16 ± 0.12	40.97 ± 0.09	270	0.27	1.0×10^{-5}
	FSRQs	1.27 ± 0.15	42.10 ± 0.14	176	0.12	0.11
	BL Lacs	1.91 ± 0.16	40.52 ± 0.07	88	0.25	0.02

the $\log \beta_{\text{app}}^{\text{max}}$ is not correlated with $\log (M_{\text{BH}}/M_{\odot})$ because of a $p = 0.05$. While the correlations between $\log \beta_{\text{app}}^{\text{max}}$, and $\log L_{\text{Disk}}$, and $\log (L_{\text{Disk}}/L_{\text{Edd}})$ are moderately significant, the positive correlations suggest that stronger accretion disk tend to have faster apparent velocities of knots. The results indicate that the central black hole mass may not be a key parameter of a jet to generate knots and to accelerate them, while the power of accretion disk and the accretion rate is likely to be critical to the jet. Previous studies has established the blazar knot propagation disturbance to be connected with γ -ray flares, as well as the jet activities (Jorstad et al. 2001b; Marscher et al. 2010; Jorstad et al. 2013; Tanaka et al. 2015; Jorstad & Marscher 2016; Jorstad et al. 2017). In the majority of these cases, γ -ray outbursts coincide with the passage of superluminal knots through the radio core (Jorstad & Marscher 2016). In this scheme, we may find a way of the accretion disk connecting the relativistic jet. We suggest a sudden increase of accretion rate of a powerful accretion disk would generate and accelerate knots, and the propagation of knot disturbance derive jet activities and show outbursts.

4.2 The criteria of selecting VFB candidates from the *Fermi* blazars

Blazars show various observational properties, for instance, the high γ -ray luminosity. In the GeV γ -ray band, the spectrum is a superposition of different radiation mechanisms, e.g., the scattering of synchrotron photons (SSC), of the seed photons from accretion disk (Dermer & Schlickeiser 1993), of the ultraviolet seed photons from broad line region (BLR, Sikora et al. 1994), of the seed photons from dusty torus (DT, Blażejowski et al. 2000; Arbeiter et al. 2002; Sokolov & Marscher 2005) by the relativistic electrons via inverse Compton process. Therefore, sources should show difference in the spectrum if their γ -ray emission consists of different mechanisms. Ackermann et al. (2015) found that FSRQs show greater γ -ray luminosity L_{γ} and larger photon index α_{ph} than BL Lacs by analyzing the third catalog of AGNs detected by the *Fermi*-LAT (3LAC). Variation is one of the characters of blazars, Yang et al. (2022) suggests that FSRQs have larger $\log VI$ than the BL Lacs. Our results suggest that $\log \beta_{\text{app}}^{\text{max}}$ is positively correlated with both α_{ph} and $\log VI$, seen in the middle and bottom panels of Fig. 1, indicate blazar have faster apparent motion tend to have softer γ -ray spectrum and higher magnitude of variability.

For the facts that we have mentioned above, in the present work, we investigate the differences between the VLBI detected *Fermi* blazars and the rest of *Fermi* blazars through these three parameters. Our results suggest that the VFBs have larger $\log L_{\gamma}$, α_{ph} and $\log VI$ than the rest of *Fermi* blazars.

Based on the complete MOJAVE 1.5 Jy sample of AGNs, Lister et al. (2015) found that 23% of these AGNs are not detected by *Fermi* because of an instrumental selection effect and partly due to their lower Doppler boosting factors. Xiao et al. (2019) suggested that those blazars not detected by *Fermi*-LAT should be *Fermi* blazar candidates if they have large apparent velocity, we also predicted some sources to be *Fermi* blazar candidates and this prediction is proved to be true (Xiao et al. 2020) when the 4FGL released. On one side, the blazars with apparent motion detected through VLBI technique are likely to be *Fermi* γ -ray source candidates. On the other side, whether there are more blazars in the *Fermi* catalogue are VLBI candidates? There are 3437 blazars that have been identified in 4FGL_DR2, out of which 407 sources (taking 11.8%) are associated with VLBI detection and most of them are detected by MOJAVE program. The quantity of VFBs is obviously underestimated because the MOJAVE program is only dedicated to monitoring the sources in the northern sky (and the southern sky source near the equator), while *Fermi*-LAT gives all-sky observation of γ -ray emitters.

For the purpose of finding more VFBs, we explore criteria of selecting VFB candidates from 4FGL based on the $\log L_{\gamma}$, α_{ph} , and $\log VI$.

We apply *Gaussian mixture models* (GMM), which is a probabilistic model that assumes all the data points are generated from a mixture of a finite number of Gaussian distributions with unknown parameters in the package of *sklearn*, which is a software machine learning library for the *Python* (Fralely & Raftery 2002), to decompose $\log L_{\gamma}$, α_{ph} and $\log VI$ distributions as shown in the left panel of Fig. 7. The proportions of each Gaussian component of the total distribution (the hidden variables) and the mean and standard deviation of each Gaussian component are obtained through an *Expectation-Maximization* (EM) algorithm, which is an iterative algorithm. In the ‘E’ step, the initial value of the parameters or the values of the last iteration is used to calculate the posterior probability of hidden variables. In the ‘M’ step, the likelihood function is maximized to obtain the mean and standard deviation. The ‘E’ and ‘M’ steps are iterated until all the estimated parameters are converged. We apply stratified sampling with a scale of 95% to run the whole GMM process 100 times in order to increase the generalization ability of our model. *Bayesian Information Criterion* (BIC) is employed to qualify the GMM model and quantify the number of *Gaussian* components. BIC value is a criterion for model selection among a finite set of models, models with lower BIC are generally preferred. In this work, we employ two criteria, which are the lowest BIC value and $\Delta\text{BIC} > 10$ (Kass & Raftery 1995), to select the decomposition model.

The BIC result suggests a three *Gaussian* components, $N = 3$ gives the lowest BIC=4943.0 and $\Delta\text{BIC}_{32} = 12.8$, for the distribution of $\log L_{\gamma}$ of the rest of *Fermi* blazars. The distribution gives clustering

probability of 0.25 for component *Gaussian*[0], 0.32 for component *Gaussian*[1] and 0.43 for component *Gaussian*[2], see in the top-right panel of Fig. 7.

The BIC result suggests a two *Gaussian* components, $N = 2$ gives the lowest BIC=1370.1 and $\Delta\text{BIC}_{32} = 35.$, for the distribution of α_{ph} of the rest of *Fermi* blazars. The distribution gives clustering probability of 0.47 for component *Gaussian*[0] and 0.53 for component *Gaussian*[1], see in the middle-right panel of Fig. 7.

A two Gaussian components model, $N = 2$ gives the lowest BIC=3585.0 and $\Delta\text{BIC}_{32} = 17.4$, which gives clustering probability of 0.21 for component *Gaussian*[0] and 0.79 for component *Gaussian*[1], is found for $\log VI$ for the rest of *Fermi* blazars as shown in the bottom-right panel of Fig. 7.

It is shown that the VFBs are mainly enveloped by *Gaussian*[1] and *Gaussian*[2] for $\log L_{\gamma}$, are almost enveloped by *Gaussian*[0] for α_{ph} and enveloped by *Gaussian*[0] for $\log VI$. We propose that the dotted-curve envelope the ‘VFB-like’ sources, the dash-dotted curve concludes the ‘transition’ sources and the dashed-curve contains the ‘non-VFB-like’ sources and suggest that the conjunction point of the dotted-curve and dashed-curve as the boundary of selecting VFB candidates. Our calculation gives the conjunction point coordinates, $\log L_{\gamma} = 45.40 \pm 0.22$, $\alpha_{\text{ph}} = 2.24 \pm 0.01$ and $\log VI = 1.71 \pm 0.07$. There are 228 sources predicted as VFB candidates, whose luminosity, photon index and variability index are greater than their boundary, and they are listed in Tab. 3.

We notice that there are 79 VFBs (taking 19.4%) with $\log L_{\gamma} < 45.40$, 144 VFBs (taking 35.4%) with $\alpha_{\text{ph}} < 2.24$, and 142 VFBs (taking 34.9%) with $\log VI < 1.71$ corresponds to $VI = 51.29$. Thus, one should be aware that there are a significant number of VFBs with $\log L_{\gamma}$ and/or α_{ph} and/or $\log VI$ less than the boundary value that we proposed, our method and criteria is proposed for selecting more promising VFB candidates.

Among our 228 VFB candidates, there are 88 (38.6%) sources in the northern sky and 140 (61.4%) sources in the southern hemisphere. This result should help the VLBI equipment to find more blazars with jet ‘knot’ structure and monitor their kinetics in the future, especially for MOJAVE.

5 CONCLUSION

In this work, we made use of a sample of VLBI detected *Fermi* blazars to study the blazar jet and accretion disk property. We found that (1) a robust correlation between the maximum apparent velocity ($\log \beta_{\text{app}}^{\text{max}}$) and γ -ray luminosity ($\log L_{\gamma}$), and this correlation is intrinsic because the correlation still exists when we removed the Doppler beaming effect; (2) following the $\log L_{\gamma}$ vs $\log \beta_{\text{app}}^{\text{max}}$, we notice knot apparent motion is related to the jet power and a larger $\log \beta_{\text{app}}^{\text{max}}$ should correspond to a more powerful jet; we found both FSRQs and BL Lacs have $\log \beta_{\text{app}}^{\text{max}}$ correlated with the jet radiation power, however, only BL Lacs have $\log \beta_{\text{app}}^{\text{max}}$ correlated with the 5 GHz jet extended region luminosity ($\log L_{5\text{GHz}}^{\text{ext}}$), which is an indicator of jet kinetic power; (3) $\log \beta_{\text{app}}^{\text{max}}$ shows no correlation with black hole mass ($\log (M_{\text{BH}}/M_{\odot})$), while it has a moderate correlation with accretion disk luminosity ($\log L_{\text{Disk}}$) and the normalized accretion disk luminosity ($\log (L_{\text{Disk}}/L_{\text{Edd}})$). The result suggests both the power of accretion disk and the accretion rate are critical to generate and accelerate blazar knots. We suggest one way of connecting accretion disk and relativistic jet that the knots are caused by sudden increase of accretion rate of a powerful accretion disk and the propagation of knots disturbance would arise jet activities and show outbursts.

In addition, we found (1) the VFBs have differences between the rest of *Fermi* blazars on γ -ray luminosity ($\log L_{\gamma}$), γ -ray photon index (α_{ph}), and variability index ($\log VI$). The VFBs have average values of $\langle \log L_{\gamma}^{\text{VFB}} \rangle = 46.20 \pm 1.07$, $\langle \alpha^{\text{VFB}} \rangle = 2.33 \pm 0.25$, $\langle \log VI^{\text{VFB}} \rangle = 2.14 \pm 0.84$, while the average values for the rest of *Fermi* blazars are $\langle \log L_{\gamma}^{\text{R}} \rangle = 45.24 \pm 1.42$, $\langle \alpha^{\text{VFB}} \rangle = 2.21 \pm 0.30$, $\langle \log VI^{\text{VFB}} \rangle = 1.30 \pm 0.50$; (2) based on the difference of $\log L_{\gamma}$, α_{ph} and $\log VI$, we generated a criteria to select VFB candidates from the rest of *Fermi* blazars by using a *Gaussian mixture models* (GMM) method. We suggested a blazar has $\log L_{\gamma} > 45.40$, $\alpha_{\text{ph}} > 2.24$ and $\log VI > 1.71$ can be considered as VFB candidates. According to this criteria, we managed to select 228 VFBs.

ACKNOWLEDGEMENTS

We thank the support of the key laboratory for astrophysics of Shanghai. H. B, Xiao acknowledges the support from National Natural Science Foundation of China (NSFC 12203034) and from Shanghai science and Technology Fund (22YF1431500); S. H, Zhang acknowledges the support from the National Science Foundation of Shanghai (20ZR1473600); J. H, Fan acknowledges the support from the NSFC (NSFC U2031201, NSFC 11733001); Z. J, Luo acknowledges the supported by Shanghai science and Technology Fund (Grant No.20070502400). We would like to thank the MOJAVE team for the use of their precious kinematic data.

DATA AVAILABILITY

For the study presented in this work, we used the following published data: (1)4FGL, https://fermi.gsfc.nasa.gov/ssc/data/access/lat/10yr_catalog/ and 4LAC. (2)MOJAVE Program, <http://www.physics.purdue.edu/astro/MOJAVE/allsources.html>, and literature in this paper. (3)NED, <https://ned.ipac.caltech.edu/forms/byname.html>.

REFERENCES

- Abdo A. A., et al., 2010, *ApJ*, 716, 30
 Abdollahi S., et al., 2020, *ApJS*, 247, 33
 Acero F., et al., 2015, *ApJS*, 218, 23
 Ackermann M., et al., 2015, *ApJ*, 810, 14
 Ajello M., et al., 2020, *ApJ*, 892, 105
 Arbeiter C., Pohl M., Schlickeiser R., 2002, *A&A*, 386, 415
 Blandford R. D., Koeningl A., 1979, *Astrophys. Lett.*, 20, 15
 Błażejowski M., Sikora M., Moderski R., Madejski G. M., 2000, *ApJ*, 545, 107
 Britzen S., et al., 2008, *A&A*, 484, 119
 Cao X., Jiang D. R., 1999, *MNRAS*, 307, 802
 Cavagnolo K. W., McNamara B. R., Nulsen P. E. J., Carilli C. L., Jones C., Birzan L., 2010, *ApJ*, 720, 1066
 Celotti A., Padovani P., Ghisellini G., 1997, *MNRAS*, 286, 415
 Chai B., Cao X., Gu M., 2012, *ApJ*, 759, 114
 Cohen M. H., Cannon W., Purcell G. H., Shaffer D. B., Broderick J. J., Kellermann K. I., Jauncey D. L., 1971, *ApJ*, 170, 207
 Cohen M. H., Lister M. L., Homan D. C., Kadler M., Kellermann K. I., Kovalev Y. Y., Vermeulen R. C., 2007, *ApJ*, 658, 232
 Dermer C. D., Schlickeiser R., 1993, *ApJ*, 416, 458
 Fan J.-H., 2002, *PASJ*, 54, L55
 Fan J.-H., Yang J.-H., Pan J., Hua T.-X., 2011, *Research in Astronomy and Astrophysics*, 11, 1413

Table 3. The superluminal *Fermi* blazar candidates

4FGL Name	Class	z	Flux1000 photon · cm ⁻² · s ⁻¹	log L_γ erg · cm ⁻² · s ⁻¹	α_{ph}	<i>VI</i>
4FGL J0001.5+2113	fsrq	1.106	1.36E-09	46.74	2.66	1564.42
4FGL J0004.4-4737	fsrq	0.88	4.36E-10	45.99	2.37	139.12
4FGL J0010.6-3025	fsrq	1.19	3.49E-10	46.24	2.46	91.59
4FGL J0011.4+0057	fsrq	1.492	4.29E-10	46.60	2.33	71.98
4FGL J0016.2-0016	fsrq	1.57631	4.17E-10	46.68	2.74	82.14

*column (1) gives the 4FGL name; column (2) gives the classification; column (3) gives the redshift; column (4) gives the integral photon flux from 1 to 100 GeV; column (5) gives the γ -ray luminosity; column (6) gives the photon spectral index; column (7) gives the variability index.

Only five items are listed, this table is available in its entirety in machine-readable forms.

- Fan J.-H., Yang J.-H., Liu Y., Zhang J.-Y., 2013, *Research in Astronomy and Astrophysics*, **13**, 259
- Fan J.-H., Bastieri D., Yang J.-H., Liu Y., Hua T.-X., Yuan Y.-H., Wu D.-X., 2014, *Research in Astronomy and Astrophysics*, **14**, 1135
- Fan J. H., et al., 2016, *ApJS*, **226**, 20
- Fan J. H., et al., 2021, *ApJS*, **253**, 10
- Fraleigh C., Raftery A. E., 2002, *Journal of the American Statistical Association*, **97**, 611
- Francis P. J., Hewett P. C., Foltz C. B., Chaffee F. H., Weymann R. J., Morris S. L., 1991, *ApJ*, **373**, 465
- Ghisellini G., Tavecchio F., 2010, *MNRAS*, **409**, L79
- Ghisellini G., Padovani P., Celotti A., Maraschi L., 1993, *ApJ*, **407**, 65
- Ghisellini G., Tavecchio F., Maraschi L., Celotti A., Sbarrato T., 2014, *Nature*, **515**, 376
- Gültekin K., et al., 2009, *ApJ*, **698**, 198
- Gupta A. C., et al., 2016, *MNRAS*, **458**, 1127
- Jorstad S., Marscher A., 2016, *Galaxies*, **4**, 47
- Jorstad S. G., Marscher A. P., Mattox J. R., Wehrle A. E., Bloom S. D., Yurchenko A. V., 2001a, *ApJS*, **134**, 181
- Jorstad S. G., Marscher A. P., Mattox J. R., Aller M. F., Aller H. D., Wehrle A. E., Bloom S. D., 2001b, *ApJ*, **556**, 738
- Jorstad S. G., et al., 2005, *AJ*, **130**, 1418
- Jorstad S. G., et al., 2013, *ApJ*, **773**, 147
- Jorstad S. G., et al., 2017, *ApJ*, **846**, 98
- Kaspi S., Smith P. S., Netzer H., Maoz D., Jannuzi B. T., Giveon U., 2000, *ApJ*, **533**, 631
- Kass R. E., Raftery A. E., 1995, *Journal of the American Statistical Association*, **90**, 773
- Kellermann K. I., 2003, in Zensus J. A., Cohen M. H., Ros E., eds, *Astronomical Society of the Pacific Conference Series Vol. 300, Radio Astronomy at the Fringe*. p. 185 ([arXiv:astro-ph/0304165](https://arxiv.org/abs/astro-ph/0304165))
- Kellermann K. I., Pauliny-Toth I. I. K., 1969, *ApJ*, **155**, L71
- Kellermann K. I., et al., 2004, *ApJ*, **609**, 539
- Kellermann K. I., et al., 2007, *Ap&SS*, **311**, 231
- Komatsu E., et al., 2011, *ApJS*, **192**, 18
- Lioudakis I., Hovatta T., Huppenkothen D., Kiehlmann S., Max-Moerbeck W., Readhead A. C. S., 2018, *ApJ*, **866**, 137
- Lister M. L., et al., 2009, *AJ*, **138**, 1874
- Lister M. L., et al., 2013, *AJ*, **146**, 120
- Lister M. L., Aller M. F., Aller H. D., Hovatta T., Max-Moerbeck W., Readhead A. C. S., Richards J. L., Ros E., 2015, *ApJ*, **810**, L9
- Lister M. L., Aller M. F., Aller H. D., Hodge M. A., Homan D. C., Kovalev Y. Y., Pushkarev A. B., Savolainen T., 2018, *ApJS*, **234**, 12
- Lister M. L., et al., 2019, *ApJ*, **874**, 43
- Lister M. L., Homan D. C., Kellermann K. I., Kovalev Y. Y., Pushkarev A. B., Ros E., Savolainen T., 2021, *ApJ*, **923**, 30
- Marscher A. P., et al., 2010, *ApJ*, **710**, L126
- McLure R. J., Dunlop J. S., 2001, *MNRAS*, **327**, 199
- McLure R. J., Dunlop J. S., 2004, *MNRAS*, **352**, 1390
- Meyer E. T., Fossati G., Georgantopoulos M., Lister M. L., 2011, *ApJ*, **740**, 98
- Nolan P. L., et al., 2012, *ApJS*, **199**, 31
- Paliya V. S., Domínguez A., Ajello M., Olmo-García A., Hartmann D., 2021, *ApJS*, **253**, 46
- Pei Z.-Y., Fan J.-H., Liu Y., Yuan Y.-H., Cai W., Xiao H.-B., Lin C., Yang J.-H., 2016, *Ap&SS*, **361**, 237
- Pei Z.-Y., Fan J.-H., Bastieri D., Sawangwit U., Yang J.-H., 2019, *Research in Astronomy and Astrophysics*, **19**, 070
- Pei Z., Fan J., Bastieri D., Yang J., Xiao H., 2020, *Science China Physics, Mechanics, and Astronomy*, **63**, 259511
- Peterson B. M., et al., 1999, *ApJ*, **510**, 659
- Peterson B. M., et al., 2000, *ApJ*, **542**, 161
- Piner B. G., Edwards P. G., 2014, *ApJ*, **797**, 25
- Piner B. G., Edwards P. G., 2018, *ApJ*, **853**, 68
- Piner B. G., Mahmud M., Fey A. L., Gospodinova K., 2007, *AJ*, **133**, 2357
- Piner B. G., et al., 2012, *ApJ*, **758**, 84
- Rawlings S., Saunders R., 1991, *Nature*, **349**, 138
- Readhead A. C. S., 1994, *ApJ*, **426**, 51
- Rees M. J., 1966, *Nature*, **211**, 468
- Scarpa R., Falomo R., 1997, *A&A*, **325**, 109
- Shaw M. S., et al., 2012, *ApJ*, **748**, 49
- Shen Y., et al., 2011, *ApJS*, **194**, 45
- Sikora M., Begelman M. C., Rees M. J., 1994, *ApJ*, **421**, 153
- Sokolov A., Marscher A. P., 2005, *ApJ*, **629**, 52
- Tan C., Xue R., Du L.-M., Xi S.-Q., Wang Z.-R., Xie Z.-H., 2020, *ApJS*, **248**, 27
- Tanaka Y. T., et al., 2015, *ApJ*, **799**, L18
- Taylor G. B., Vermeulen R. C., Readhead A. C. S., Pearson T. J., Henstock D. R., Wilkinson P. N., 1996, *ApJS*, **107**, 37
- Urry C. M., Padovani P., 1995, *PASP*, **107**, 803
- Vermeulen R. C., Readhead A. C. S., Backer D. C., 1994, *ApJ*, **430**, L41
- Vestergaard M., 2002, *ApJ*, **571**, 733
- Vestergaard M., Peterson B. M., 2006, *ApJ*, **641**, 689
- Villata M., et al., 2006, *A&A*, **453**, 817
- Weaver Z. R., et al., 2022, *ApJS*, **260**, 12
- Willott C. J., Rawlings S., Blundell K. M., Lacy M., 1999, *MNRAS*, **309**, 1017
- Wills B. J., Wills D., Breger M., Antonucci R. R. J., Barvainis R., 1992, *ApJ*, **398**, 454
- Xiao H. B., Pei Z. Y., Xie H. J., Hao J. M., Yang J. H., Yuan Y. H., Liu Y., Fan J. H., 2015, *Ap&SS*, **359**, 39
- Xiao H., et al., 2019, *Science China Physics, Mechanics, and Astronomy*, **62**, 129811
- Xiao H., Fan J., Rando R., Zhu J., Hu L., 2020, *Astronomische Nachrichten*, **341**, 462
- Xiao H., Ouyang Z., Zhang L., Fu L., Zhang S., Zeng X., Fan J., 2022, *ApJ*, **925**, 40
- Xie G. Z., Liu F. K., Liu B. F., Lu R. W., Li K. H., Zhu Y. Y., 1991, *A&A*, **249**, 65
- Xiong D. R., Zhang X., 2014, *MNRAS*, **441**, 3375
- Yang W.-X., Xiao H.-B., Wang H.-G., Yang J.-H., Pei Z.-Y., Wu D.-X., Yu-Hai Y., Fan J., 2022, *Research in Astronomy and Astrophysics*
- Zhang Y.-W., Fan J.-H., 2008, *Chinese J. Astron. Astrophys.*, **8**, 385
- Zhang J., Liang E.-W., Zhang S.-N., Bai J. M., 2012, *ApJ*, **752**, 157

Zhang L., Chen S., Xiao H., Cai J., Fan J., 2020, *ApJ*, 897, 10

This paper has been typeset from a $\text{\TeX}/\text{\LaTeX}$ file prepared by the author.

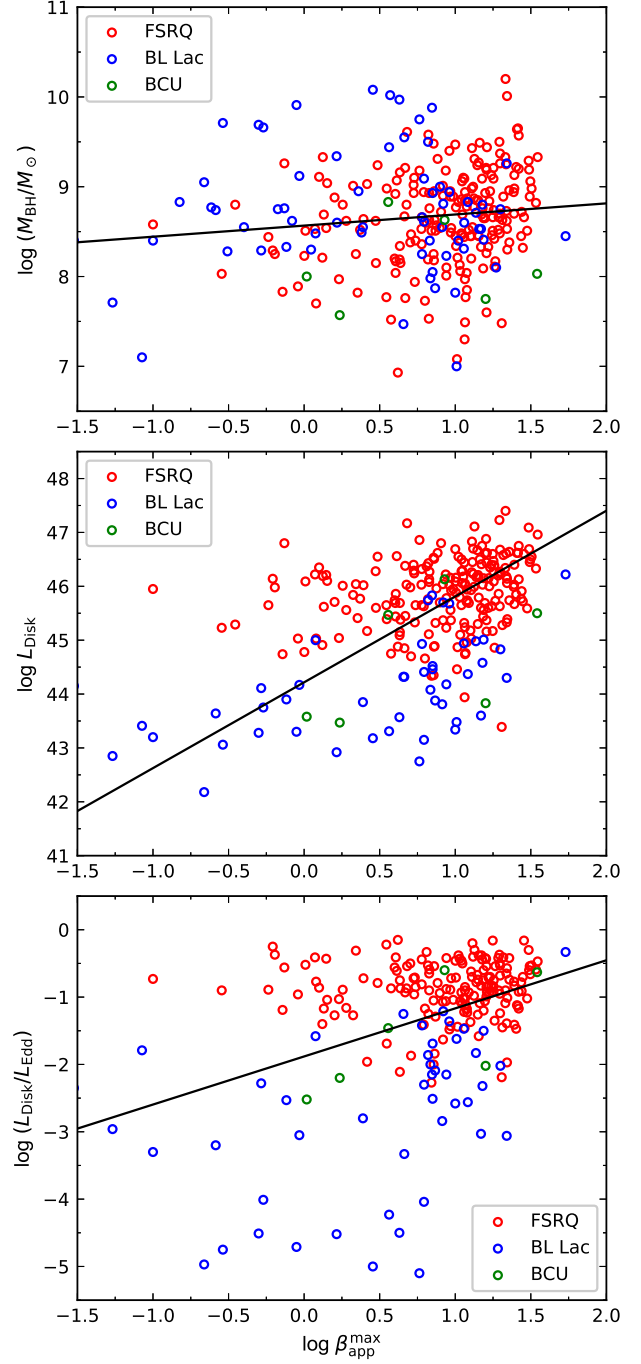


Figure 2. The correlations of $\log (M_{\text{BH}}/M_{\odot})$, $\log L_{\text{Disk}}$, and $\log (L_{\text{Disk}}/L_{\text{Edd}})$ against $\log \beta_{\text{app}}^{\text{max}}$ for the VFBS. The FSRQs in red, the BL Lacs in blue, and the BCUs in green.

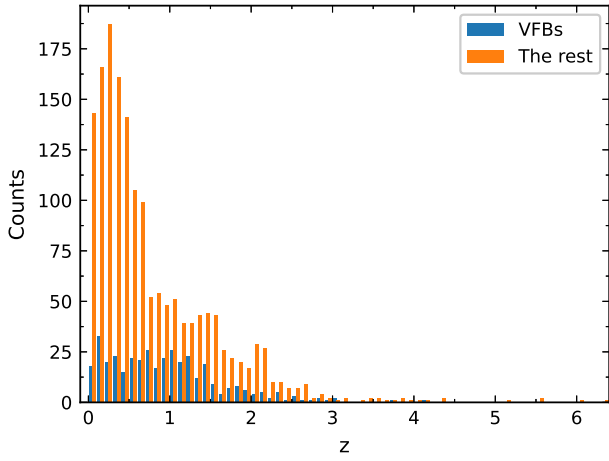


Figure 3. The redshift z distribution for the VFBS (the blue bar) and the rest of *Fermi* blazars (the orange bar).

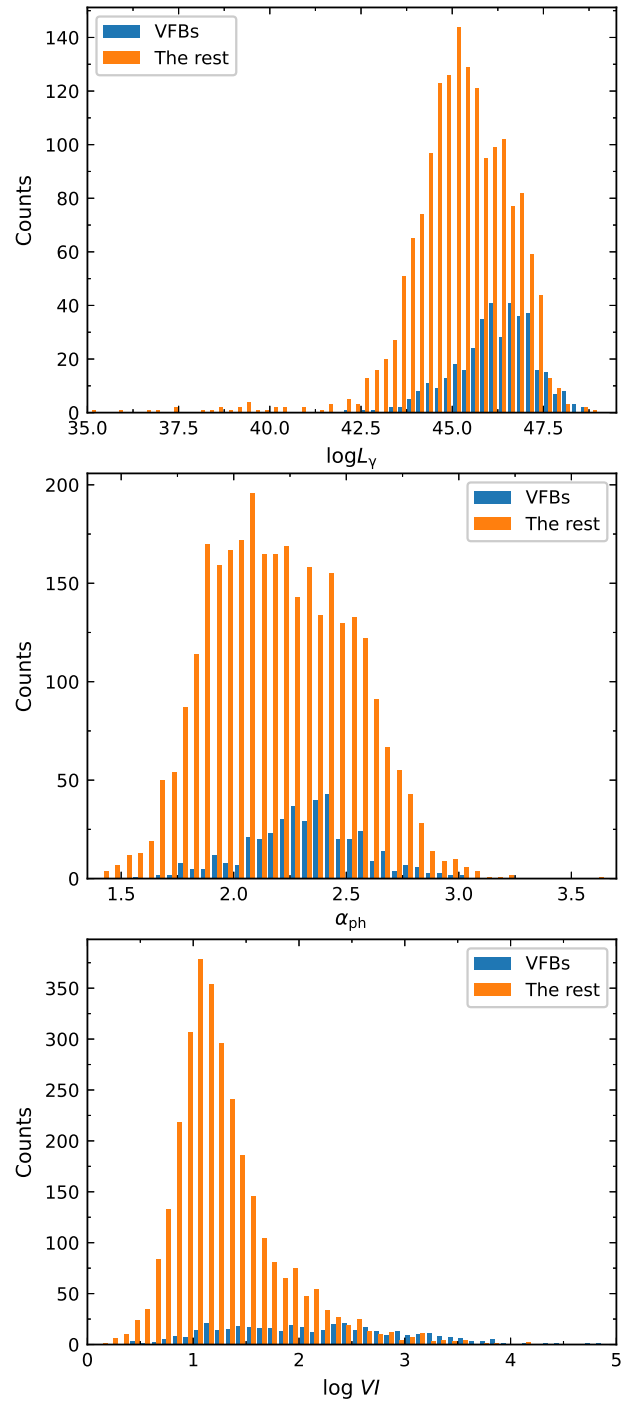


Figure 4. The $\log L_\gamma$, α_{ph} and $\log VI$ distribution for the VFBS (the blue bar) and the rest of *Fermi* blazars (the orange bar).

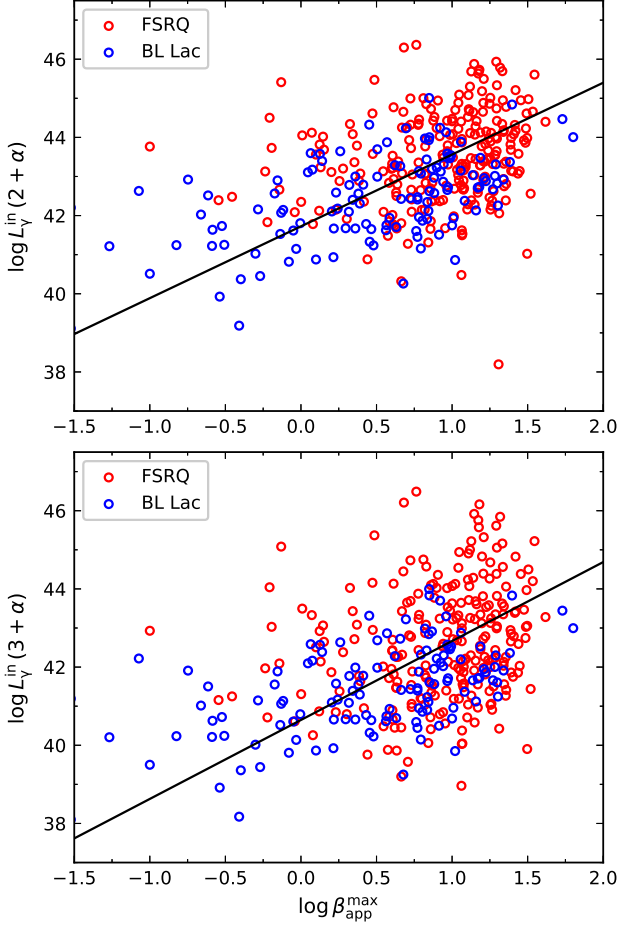


Figure 5. The correlations of intrinsic $\log L_{\gamma}^{\text{in}}$ against $\log \beta_{\text{app}}^{\text{max}}$ for the VFBs. The FSRQs in red and the BL Lacs in blue.

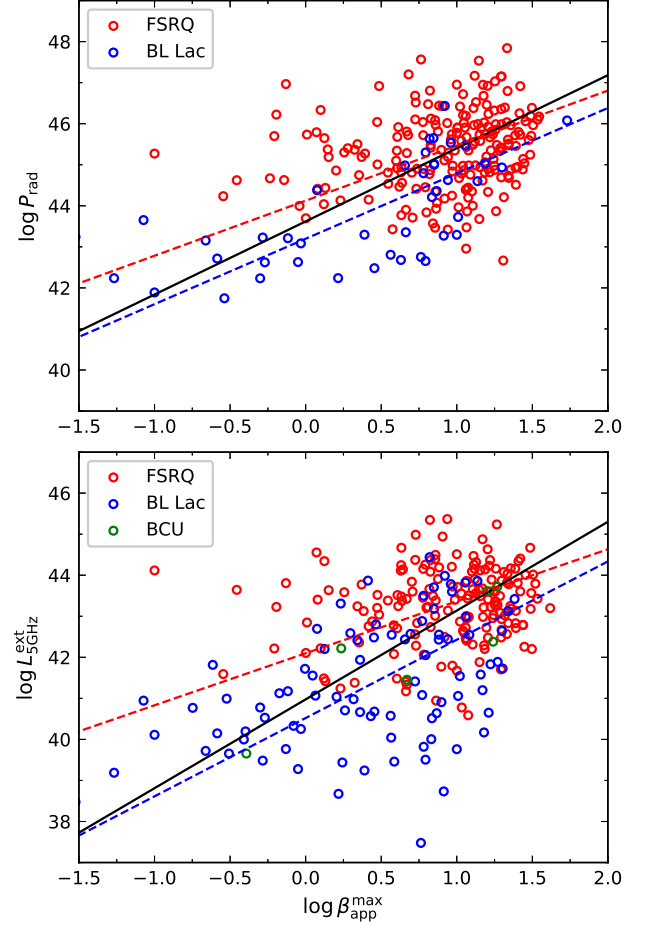


Figure 6. The correlations of $\log P_{\text{rad}}$ and $\log L_{5\text{GHz}}^{\text{ext}}$ against $\log \beta_{\text{app}}^{\text{max}}$ for the VFBs. The FSRQs in red, the BL Lacs in blue, and the BCUs in green.

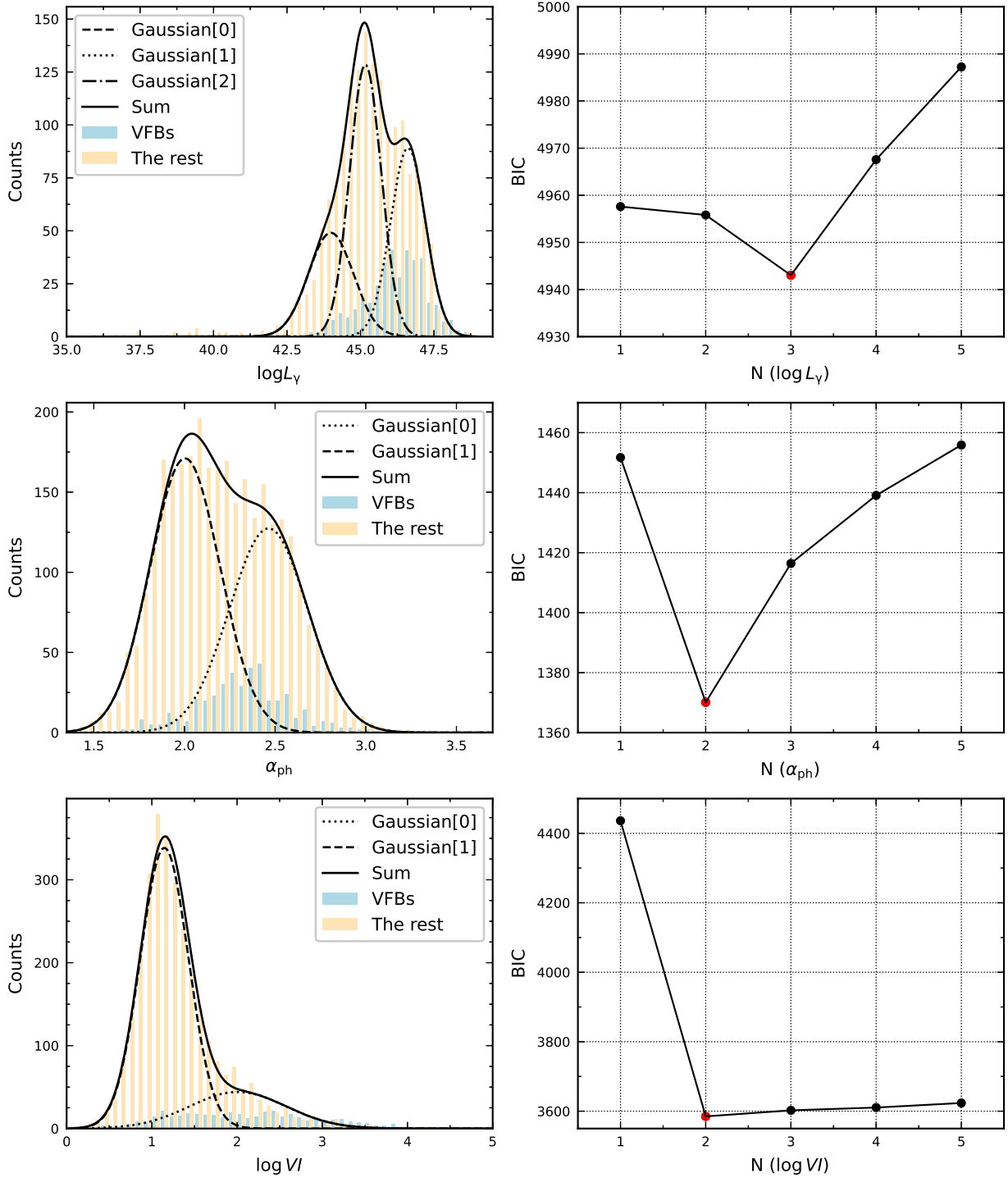


Figure 7. The distributions of γ -ray luminosity ($\log L_\gamma$), photon index (α_{ph}) and variability index ($\log VI$) that fitted with GMM. The blue bar stands for the VFBs, the orange bar stands for the rest of *Fermi* blazars.